Environ Geochem Health (2024) 46:246
https://doi.org/10.1007/s10653-024-02007-1

ORIGINAL PAPER

# One-pot synthesis of g-$C_3N_4$/N-doped $CeO_2$ nanocomposites and their potential visible light-driven photocatalytic degradation of methylene blue dye

**A. S. Karthik · Smita Agrawal · S. Senthil · Abhijit Debnath · Sandhanasamy Devanesan · Ahmed E. A. Zohier · S. Vignesh**

Received: 5 March 2024 / Accepted: 22 April 2024 / Published online: 12 June 2024


**Abstract** In the pursuit of efficient photocatalytic materials for environmental applications, a new series of g-$C_3N_4$/N-doped $CeO_2$ nanocomposites (g-$C_3N_4$/N-$CeO_2$ NCs) was synthesized using a straightforward dispersion method. These nanocomposites were systematically characterized to understand their structural, optical, and chemical properties. The photocatalytic performance of g-$C_3N_4$/N-$CeO_2$ NCs was evaluated by investigating their ability to degrade methylene blue (MB) dye, a model organic pollutant. The results demonstrate that the integration of g-$C_3N_4$ with N-doped $CeO_2$ NCs reduces the optical energy gap compared to pristine N-doped $CeO_2$, leading to enhanced photocatalytic efficiency. It is benefited from the existence of g-$C_3N_4$/N-$CeO_2$ NCs not only in promoting the charge separation and inhibits the fast charge recombination but also in improving photocatalytic oxidation performance. Hence, this study highlights the potential of g-$C_3N_4$/N-$CeO_2$ NCs as promising candidates for various photocatalytic applications, contributing to the advancement of sustainable environmental remediation technologies.

**Keywords** g-$C_3N_4$/N-$CeO_2$ NCs · Methylene blue dye · Photocatalytic degradation · Band gap · Solar light

A. S. Karthik · S. Senthil (✉)
Department of Chemistry, Government Arts College (A), Salem, Tamilnadu 636007, India
e-mail: shendils@gmail.com

A. S. Karthik
Department of Chemistry, Arignar Anna Government Arts College, Attur, Tamilnadu 636121, India

S. Agrawal
Department of Horticulture, Rajmata Vijayaraje Scindia Krishi Vishwa Vidyalaya, Gwalior, Madhya Pradesh 474002, India

A. Debnath
Department of Horticulture, Krishi Vigyan Kendra, Dhalai, Tripura 799278, India

S. Devanesan
Department of Physics and Astronomy, College of Science, King Saud University, P. O. Box 2455, 11451 Riyadh, Saudi Arabia

A. E. A. Zohier
Department of Science Technology and Innovation Unit, King Saud University, P. O. Box-2454, 11451 Riyadh, Saudi Arabia

S. Vignesh
Department of Applied Chemistry, Saveetha School of Engineering, Saveetha Institute of Medical and Technical Sciences, Saveetha University, Chennai, Tamil Nadu 602105, India

S. Vignesh
School of Chemical Engineering, Yeungnam University, 280 Daehak-Ro, Gyeongsan 38541, Republic of Korea

## Introduction

In the wood and textile industries, the cationic dyes such as Methylene Blue (MB) are largely used with various applications (Nas et al., 2019; Abbasi et al. 2012). Generally MB, present in aquatic medium causes irreparable harms to water bodies. The degradation of MB from wastewater is a major issue because MB degraded unevenly leads to the formation of hazardous chemical species, finally affecting the environment. Reactive oxygen and other strong oxidative species are necessary for the efficient breakdown of organic contaminants. In order to solve environmental issues, heterogeneous photocatalysts must be used in conjunction with sustainable energy sources like solar energy. Pollutants may be effectively broken down into mineralized species like $H_2O$ and $CO_2$ by an effective advanced oxidation process called solar light-assisted photocatalysis (Huang et al., 2018; Liying et al. 2013; Malathy et al. 2023). Although photocatalysts with attractive properties, such as $TiO_2$, ZnO, and CdS, have long been preferred (Akpan & Hameed, 2009; Rajendran et al., 2022), even though the familiar catalysts have bottleneck drawbacks, including low utilization visible light poitions and high electron–hole charge recombination rates. One well-known rare earth metal oxide that is useful as a photocatalyst for breaking down organic dyes is cerium ($CeO_2$). Its capacity to store oxygen and convert $Ce^{4+}$ to $Ce^{3+}$ accounts for its high catalytic efficiency (Dey et al., 2022; Manimegalai et al., 2023; Ranjith et al., 2023; Xu et al. 2012). Cerium oxide seems to be titanium dioxide in the basis of basic phoptocatalytic qualities like environmentally friendly, inexpensive, and chemically inert. $CeO_2$ also responds more readily to visible light in the solar spectrum than $TiO_2$ does (Gao et al., 2013; Rajendran et al., 2024; Thangavelu et al., 2023). But problems like the recombination of photogenerated charges ($e^-$ and $h^+$) and the insufficient catalytic surface of $CeO_2$ severely limit its photocatalytic activity.

g-$C_3N_4$ is a heterocyclic organic semiconductor that has remarkable chemical-based and thermal conductivity. Considering that it responds to visible light, its low cost and broad distribution make it a desirable alternative. It can be paired with broad band gap photocatalysts because of this property (Dey et al., 2022). Scholars have emphasized the noteworthy influence of the non-toxic carbon nitride semiconductor g-$C_3N_4$ in diverse domains, including organic pollutant degradation, water splitting, and biosensors (Gao et al., 2013; Rajendran et al., 2024; Thangavelu et al., 2023; Muthamilarasu et al. 2022; Wetchakun et al. 2012), therefore establishing it as a prominent participant in the field of environmental pollutant degradation research. Notwithstanding its encouraging attributes, g-$C_3N_4$ encounters obstacles that impact its catalytic efficacy. Its further growth is hampered by problems such high photogenerated charge carrier recombination, subpar surface qualities, and restricted solar light absorption, especially below the 460 nm absorbance maximum (Gao et al., 2013; Thangavelu et al., 2023). To effectively utilize g-$C_3N_4$, it is imperative to address these deficiencies. To overcome these obstacles, scientists have combined g-$C_3N_4$ with oxide semiconductors such as CuO, ZnO, and others to create binary or multinary nanocomposites (Chandrasekar et al., 2023; Malathi et al., 2024; Divya et al. 2021; Li et al. 2009). After formation of g-$C_3N_4$ coupled oxide semiconductors the photocatalytic activity shifted next milestone due to its enhanced optical and photophysical characteristics. They are therefore more effective in breaking down stable organic contaminants.

In order to overcome the restricted photocatalytic capabilities of materials with $CeO_2$ and g-$C_3N_4$, scientists have investigated appropriate heterojunction building techniques. These methods seek to enhance important catalytic characteristics, such as the efficient separation of photogenerated electrons and holes and the effective use of visible light. The selection of a synthetic procedure is critical in order to achieve desired properties like high surface area and excellent crystallinity. Hydrothermal and co-pyrolysis techniques are becoming popular ways to fabricate carbon allotrope copupled metaloxodes nanocomposites (Liu et al., 2015; Malathi et al., 2023). Huang et al.'s work (Runda et al., 2021) used the creation of a unique $CeO_2$/g-$C_3N_4$ composite to show how successful this method is. Their results demonstrated that the combination of $CeO_2$ and Ag-GCN produced remarkable photocatalytic activity for the degradation of the dyes AY-36 and DR-12. The present study highlights the significance of heterojunction assembly techniques in augmenting the photocatalytic efficacy of substances based on g-$C_3N_4$ and $CeO_2$. The study made a number of noteworthy observations, such as the remarkable adsorption capacities of both catalysts and dyes, the excellent absorption of visible light, and the efficient conversion of reactive oxygen species. Furthermore, in $CeO_2$/g-$C_3N_4$ composites, Nachimuthu

et al. (2023) noted particular photocatalytic features such a wide surface area and regulated shape.

In this work, the creation of g-$C_3N_4$/N-doped $CeO_2$ nanocomposites offers a viable solution to the environmental problems brought on by the breakdown of organic pollutants. These nanocomposites provide increased photocatalytic activity by using solar light irradiation, possibly circumventing the drawbacks of conventional photocatalysts. This work intends to clarify the structural and photocatalytic characteristics of these innovative nanocomposites using a combination of XRD, SEM, and UV–vis DRS studies, opening the door for their potential use in environmental remediation.

## Materials and methods

### Materials

For the synthesis of the parent photocatalyst, aqueous ammonia (28–30%) was acquired from Merck India, while urea and $(NH_4)_2Ce(NO_3)_6$ were procured from Loba Chemie India. The water used to make all of the solutions was double-distilled. NaOH and HCl were used to alter the pH, while benzoquinone (BQ), triethanolamine (TEOA), and isopropyl alcohol (IPA) were used as scavengers for measuring the active species.

Methylene blue dye (MB) was used for photocatalytic degradation studies.

Chemical formula: $C_{16}H_{18}ClN_3S$.

Molecular weight: 319. 85 g/mol.

Water solubility: 43. 6 g/L in water at 25 °C.

$\lambda_{max}$: 668 nm.

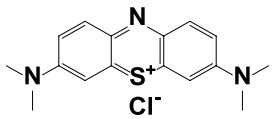


Methylene Blue (Phenothiazin- 5-ium, 3,7-bis(dimethylamino)-, chloride)

### Methods

#### *Formation of g-$C_3N_4$ sheet*

Pyrolysis was used in the deammoniation process to create the g-$C_3N_4$ sheet. The conventional protocol involved dissolving 15 g of urea in 50 mL of double-distilled water and agitating the mixture for 30 min to achieve homogeneity. After that, the urea solution was dried in a hot air furnace at 100 °C to eliminate any remaining water. The dried urea was then heated to 200 °C for 2 h, and then it was subjected to a solid-phase reaction in a traditional muffle furnace for 2 h at a ramp rate of 10 °C per minute at 450 °C. The result was a pale yellow solid known as the bare g-$C_3N_4$ sheet, which was produced after cooling to room temperature.

#### *Synthesis of N-doped $CeO_2$ nanoparticles*

The following protocol was used in order to synthesize N-doped $CeO_2$ nanoparticles (Xiaolong et al., 2017): First, a suitable volume of double-distilled water was used to dissolve 5 g of $(NH_4)_2Ce(NO_3)_6$ (CAN), which was then thoroughly agitated until total uniformity was attained. The CAN solution was then mixed with 10 mL of ammonia solution dropwise to create a gel. Following filtering and a wash with an aqueous-alcoholic solution, the gel was treated with 0.009 M% urea. After that, surplus water and contaminants were removed from the nitrogen-impregnated cerium hydroxide gel by heating it for 12 h at 120 °C. Ultimately, the dehydrated powder underwent calcination in a muffle furnace at 500 °C to produce finely distributed N-doped $CeO_2$ nanoparticles.

#### *Fabrication of N-doped $CeO_2$/g-$C_3N_4$nanocomposites*

N-doped $CeO_2$/g-$C_3N_4$ NCs were first created by dispersing 100 mg of g-$C_3N_4$ in 50 mL of double-distilled water and ultrasonically dissolving it for 2 h. The dispersing solution was then combined with 900 mg of N-doped $CeO_2$, and the combination was agitated for a duration of 12 h. Following separation, the composite substances were dried at 80 °C and then treated for 3 h at 300 °C. Various aggregates were additionally made, ranging from 0.90:0.10 to 0.70:0.30 and 0.60:0.10, respectively, with varying mass ratios and concentrations of N-doped $CeO_2$ and g-$C_3N_4$.

#### *Characterization*

Using Cu K radiation ($\lambda = 1.05466$), powder X-ray diffraction (XRD) examination was performed

with a Bruker D8 Advanced diffractometer. Utilizing a Bruker VECTOR 22 spectrometer, Fourier-transform infrared (FT-IR) spectra were obtained. Using an S-5000 device from Hitachi Ltd., surface characteristics and the crystalline framework were examined using scanning electron microscopy (SEM). Approaches for transmission electron microscopy (TEM) were used with a JEM 2100F device from JEOL Inc. A UV–Vis–NIR spectrophotometer (Varian/carry 5000) was used to quantify optical absorbing capacity, and a Jobin Yvon FLUOROLOG-FL3-11 spectrometer was used to acquire photoluminescence (PL) spectra.

*Photocatalytic experiments*

The model contaminant used to assess the composites photocatalytic capabilities was methylene blue (MB) dye. In order to conduct the investigation, a 100 mL solution holding 30 ppm of MB dye had to be prepared. Next, 300 mg of catalyst had to be added. Next, a magnetic stirrer was used to agitate the mixture. The solution that contained the dye was incubated in the dark for 30 min before being exposed to sunlight. The dye solution was then removed, and a 4 mL sample was separated. Using a Perkin Elmer Lambda 25 UV–visible spectrophotometer, wavelengths of absorption were captured. The aforementioned equation was used to calculate the percentage degradation (Yang et al., 2012):

$$\% \, D = \frac{C_o - C_t}{C_o} \times 100 \quad (1)$$

where $C_t$ denotes the color absorbing with a catalyst following a certain amount of time, and $C_o$ denotes the color uptake without catalyst.

## Results and discussion

X-ray diffraction analysis

X-ray diffraction (XRD) analysis was used to look at the generated photocatalysts crystallization characteristics. The XRD patterns of g-$C_3N_4$, N-doped $CeO_2$, and g-$C_3N_4$/N-doped $CeO_2$ nanocomposites (g-$C_3N_4$/N-$CeO_2$ NCs) are shown in Fig. 1. The diffraction

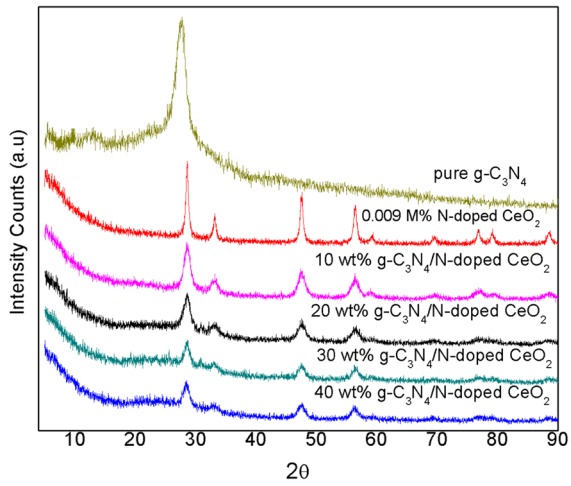


**Fig. 1** XRD patterns of the as-prepared N-doped $CeO_2$ nanoparticles, g-$C_3N_4$ and g-$C_3N_4$/N-$CeO_2$ NCs

peaks shown at 28.3°, 32.8°, 47.2°, 56.1°, and 69.3° in Fig. 1 are ascribed to the N-doped $CeO_2$ nanoparticles cubic fluorite crystalline phase, which resembles the pattern of pure $CeO_2$ very closely (JCPDF No. 34–0394).

The naked g-$C_3N_4$ has a peculiar diffraction pattern; a clear peak is seen at 27.4°, which corresponds to crystalline planes that look like (002). This diffraction pattern is exactly matches with normal JCPDS card No. 87–1526. The necessity diffraction patterns of g-$C_3N_4$ and N-doped $CeO_2$ nanoparticle are clearly seen in the g-$C_3N_4$/N-$CeO_2$ nanocomposites pattern. This is demonstrates that g-$C_3N_4$ and N-doped $CeO_2$ have been successfully fabricated. Furthermore, the creation of the composites is shown by a minor shift in the higher 2θ value, indicating a significant interaction between g-$C_3N_4$ and N-doped $CeO_2$. In addition increase the loading of g-$C_3N_4$ content on N-doped $CeO_2$ surface, the crystallanity of -$C_3N_4$/N-$CeO_2$ NCs were decreased which is due to over incorporation of $C_3N_4$ content on N-doped $CeO_2$. Furthermore, no aberrant peaks other than those corresponding to N-doped $CeO_2$ and g-$C_3N_4$ are detected.

Scanning electronic microscopic and EDX analysis

The surface microstructure and their nanostructure of g-$C_3N_4$, N-doped $CeO_2$, and g-$C_3N_4$/N-doped $CeO_2$

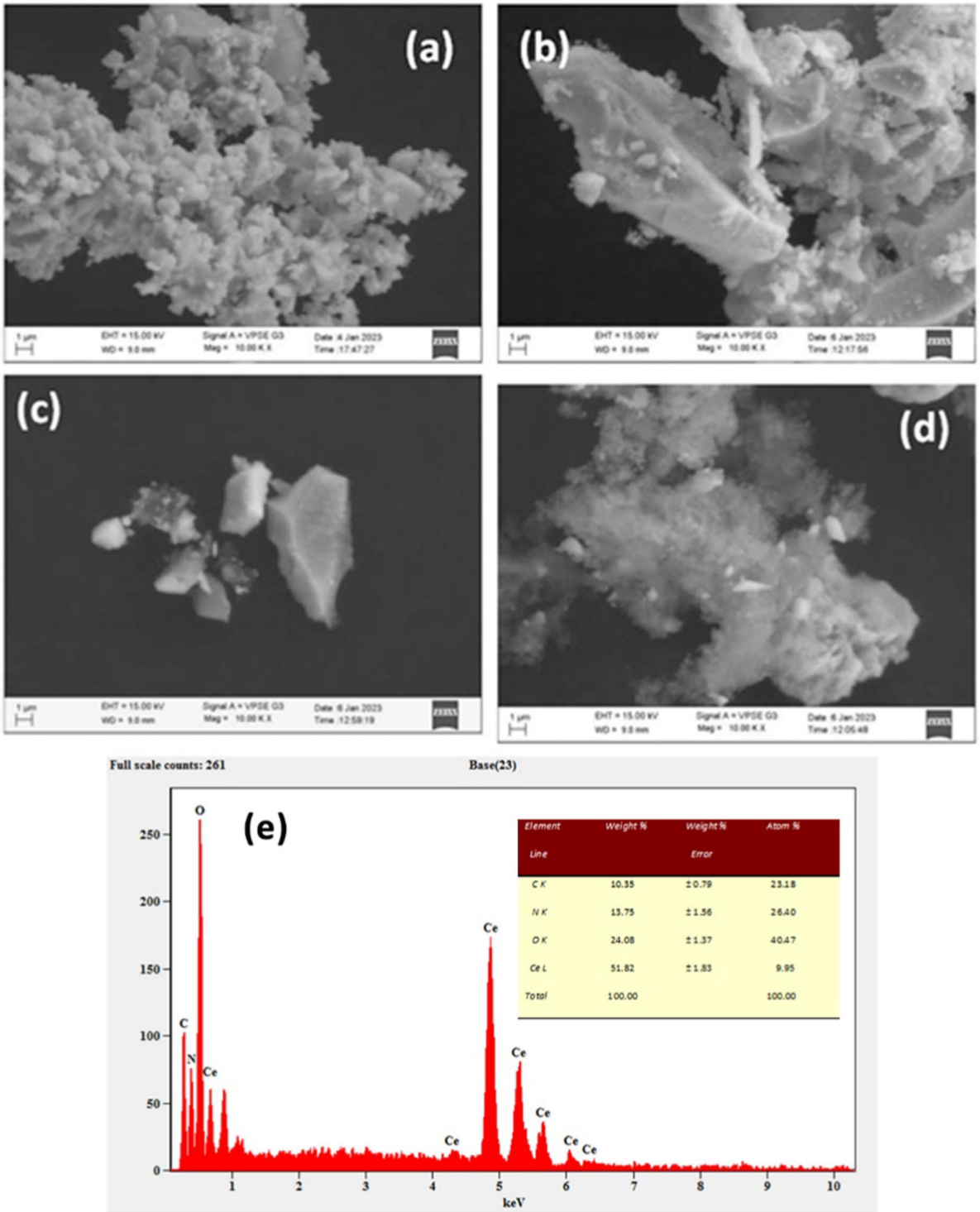


**Fig. 2** SEM images of the as-prepared **a** g-$C_3N_4$ **b** N-doped $CeO_2$, **c** 10 wt% g-$C_3N_4$/N-$CeO_2$ NCs **d** 30 g-$C_3N_4$/N-$CeO_2$ NCs **e** EDX of g-$C_3N_4$/N-$CeO_2$ nanocomposites

nanocomposites with 10 wt% and 30 wt% loading were investigated by SEM examination. It is possible to detect g-$C_3N_4$ as a fluffy, sheet-like structure in Fig. 2a. The erratically aggregating amorphous nanoparticles of N-doped $CeO_2$ produced by the sol–gel technique are shown in Fig. 2b.

The SEM representation of the 10 weight percent g-$C_3N_4$/N-$CeO_2$ nanocomposites is shown in Fig. 2c. It demonstrates two tightly packed particles with comparable shape, indicating that the nanocomposites comprising g-$C_3N_4$ and N-doped $CeO_2$ were successfully formed. In the interim, Fig. 2d depicts the surface microstructure of 30 weight percent g-$C_3N_4$/N-$CeO_2$ nanocomposites, which clearly exhibits a nanosponge-like structure. This particular structure may have improved textile dye absorption properties.

The elemental composition of g-$C_3N_4$/N-doped $CeO_2$ nanocomposites is determined by EDX, a micro analytical technique used in association with SEM. The EDX detects X-rays emitted from sample when electrons are bombarded on material surface. Data about chemical composition is provided by measuring the intensity and energy of the signal. The EDX spectrum shows frequency of X-rays in counts for each energy level. The intensity of the peak gives information about the amount of the element in sample [41]. Figure 2e represents EDX spectra of g-$C_3N_4$/N-doped $CeO_2$ nanocomposites. The weight percentage of Ce, O, C and N elements present in the appropriate amounts like 51.82, 24.08, 10.35 and 13.75 wt% respectively. These results indicate high amount of $CeO_2$ present in the g-$C_3N_4$/N-doped $CeO_2$ nanocomposites than the C3N4. Overall EDX result, indicates there is no unwanted impurities present in the prepared samples.

## Transmission electron microscopic analysis

The transmission electron microscopy (TEM) images of 30 weight percent g-$C_3N_4$/N-$CeO_2$ nanocomposites are shown in Fig. 3, which also shows the interaction between g-$C_3N_4$ and N-doped $CeO_2$. At 200 nm, a cloudy-based morphology with granularity of varying sizes is shown in Fig. 3b. Looking more closely in Fig. 3c, the surface of the g-$C_3N_4$/N-$CeO_2$ nanocomposites shows the presence of 20 nm-long, granular-shaped aggregates. The nano-sized crystals in Fig. 3d demonstrate the abundance of N-doped $CeO_2$ next to the g-$C_3N_4$ sheet. In addition, Fig. 3f SAED pattern for the g-$C_3N_4$/N-$CeO_2$ nanocomposites shows a ring-like pattern, which suggests that this material has less crystalline structure than the other materials. The polycrystalline

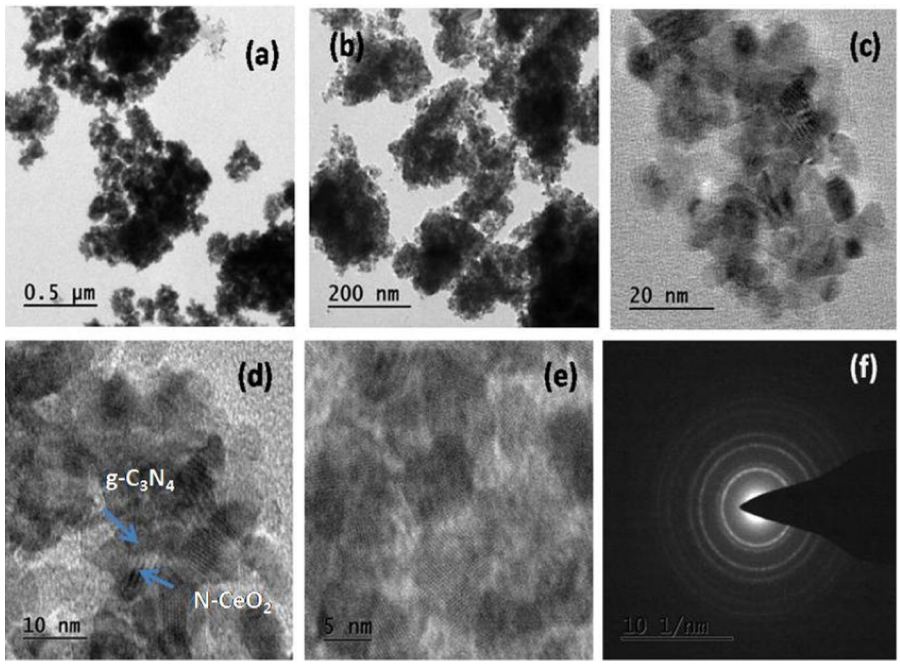


**Fig. 3** TEM image of 30 wt% g-$C_3N_4$/N-$CeO_2$ NCs

character of the nanostructures is shown by the SAED picture, which is shown as a ring in Fig. 3f. The reflecting planes that were seen and those found in the XRD data are nearly in line.

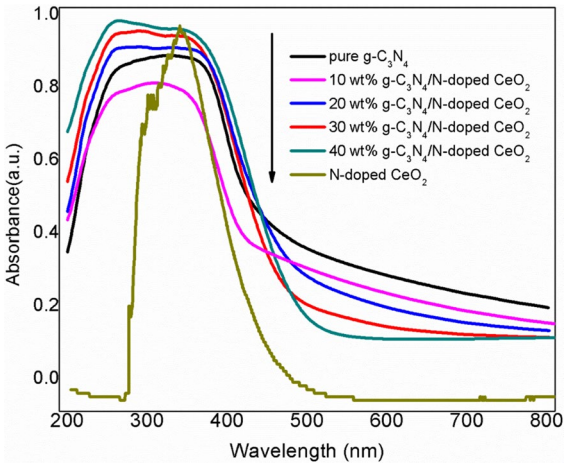


**Fig. 4** UV-DRS spectra of g-$C_3N_4$, N-doped $CeO_2$nanoparticles, and different weight ratio of g-$C_3N_4$/N-$CeO_2$ NCs

UV–visible DRS analysis

The synergistically impact of g-$C_3N_4$ on N-doped $CeO_2$ nanoparticles was investigated using UV–visible diffuse reflectance spectroscopy (DRS) investigation. This is important for comprehension of their photocatalytic characteristics, particularly in degrading organic contaminants under visible light conditions. UV–visible DRS analysis was used to measure the light absorbance of g-$C_3N_4$, N-doped $CeO_2$, and g-$C_3N_4$/N-$CeO_2$ nanocomposites, as shown in Fig. 4. In the picture, photons are absorbed up to 550 nm by the g-$C_3N_4$ sheet, whereas N-doped $CeO_2$ nanoparticles show an absorbance peak at 485 nm. Furthermore, g-$C_3N_4$/N-$CeO_2$ nanocomposites exhibit increased absorbance between 485 and 517 nm. It may be inferred from this that all g-$C_3N_4$/N-$CeO_2$ nanocomposites absorb visible light more efficiently than N-doped $CeO_2$ nanoparticles individually. The stronger relationship between g-$C_3N_4$ and N-$CeO_2$ is suggested by the greater absorption of visible light in g-$C_3N_4$/N-$CeO_2$ nanocomposites. A spectrum redshift results from reducing the interface caused by an increase in g-$C_3N_4$ concentration on N-$CeO_2$, which enhances electronic interaction between the materials. Zhiquan et al. (2020) observed that associations

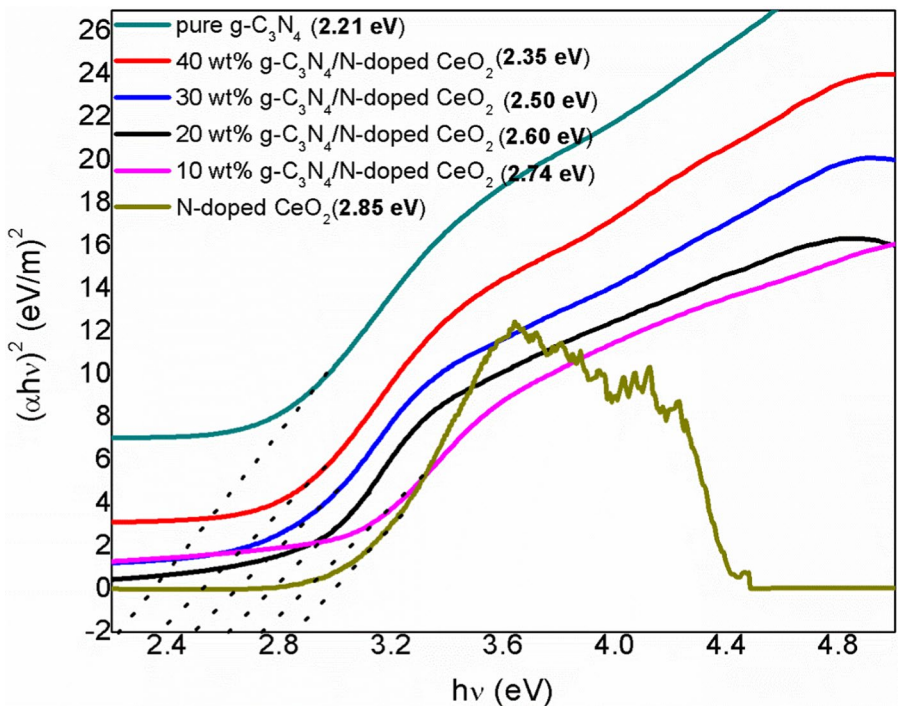


**Fig. 5** Band gap energy of g-$C_3N_4$, N-doped $CeO_2$ nanoparticles, and different weight ratio of g-$C_3N_4$/N-$CeO_2$ NCs

among materials with narrow-band gap and wide-band gap features can improve optical qualities, which is consistent with this phenomena (Fig. 5).

The produced photocatalysts energy spectrum was calculated using the formula $\alpha h\upsilon = A(h\upsilon/Eg)^{n/2}$ (Ratchnashree et al., 2023), in which α denotes the absorption coefficient, υ denotes the light frequency, Eg denotes the band gap, and h is the Planck constant. The range of band gap energies of g-$C_3N_4$, N-doped $CeO_2$ nanoparticles, and different weight percentages of g-$C_3N_4$/N-$CeO_2$ nanocomposites were calculated using this equation, and the results showed that they were around 2.85 eV, 2.21 eV, 2.74 eV, 2.60 eV, 2.50 eV, and 2.35 eV, respectively. With an increase in g-$C_3N_4$ content, it was found that the band gap potential of g-$C_3N_4$/N-$CeO_2$ nanocomposites dropped from 2.74 to 2.35 eV. This decrease in band gap energy is explained by the nanocomposites increased g-$C_3N_4$ content. Consequently, this combinatorial effect, characterized by a reduction in the band gap energy, efficiently amplifies electron–hole pair separation, resulting in enhanced absorption in the visible light spectrum.

PL analysis

The distinction of photogenerated charge carriers inside the photocatalysts is shown by the photoluminescence spectra (PL), which are crucial for evaluating the process of photocatalytic decomposition (Gomathi et al., 2023). A lower PL intensity frequently reflects a higher level of photocatalytic activity because of less electron–hole recombination. At an excitation wavelength of 375 nm, PL spectra of the produced photocatalysts were acquired. Interestingly, as Fig. 6 illustrates, N-doped $CeO_2$ nanoparticles had a greater PL peak intensity, especially in the 550 nm wavelength region. This implies that electron–hole recombination may not have been successfully suppressed by nitrogen doping within the predicted range. On the other hand, g-$C_3N_4$/N-$CeO_2$ nanocomposites showed a much smaller PL emission band.

The high interface and intimate contact between g-$C_3N_4$ and N-doped $CeO_2$ is consequently responsible for the greater effectiveness in photocatalytic decomposition, as indicated by the reduced PL emission band (Ran et al., 2019). Remarkably, the 30 weight percent composition of g-$C_3N_4$/N-$CeO_2$ nanocomposites shows the lowest

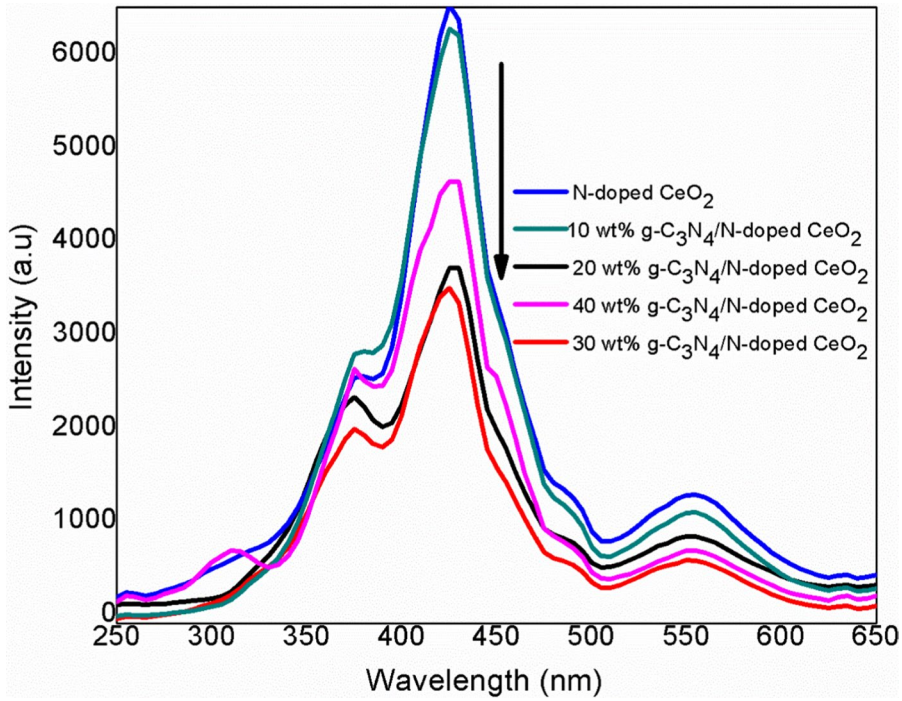


**Fig. 6** PL spectra of the N-doped $CeO_2$nanoparticles and different weight ratios of g-$C_3N_4$/N doped $CeO_2$ nanocomposites

rate of recombination of photogenerated charge carriers. The 30 wt% g-$C_3N_4$/N-$CeO_2$ nanocomposites had the lowest PL intensity when compared to other primary and nanocomposite materials. This suggests that the 30 wt% g-$C_3N_4$/N-$CeO_2$ nanocomposites effectively separate photogenerated charge carriers, hence improving the activity of photocatalytic reactions. The PL emission intensity of the 40 wt% g-$C_3N_4$/N-$CeO_2$ nanocomposites, nevertheless improves with an additional rise in g-$C_3N_4$ content to 40 wt%, indicating less efficient separation of photogenerated charge carriers than in the 30 wt% g-$C_3N_4$/N-$CeO_2$ nanocomposites.

## FT-IR analysis

Finding the molecular connections between the atoms is mostly accomplished by FT-IR analysis. We must identify the functional categories in unitary and binary photocatalysts based on the study. Figure 7 displays the g-$C_3N_4$/N-$CeO_2$ NCs and the N-doped $CeO_2$ nanoparticles of FT-IR spectra. In general, transition metal oxide ($MO_x$) exhibits an absorption band between 400 and 750 $cm^{-1}$, which is associated with vibrations in the Ce–O bond. Regarding this, the FTIR spectrum of N-doped $CeO_2$ shows a sharp peak at 703 $cm^{-1}$, which suggests that the Ce–O stretching vibration is present (Wang et al., 2019).

The band found at 813 $cm^{-1}$ in the g-$C_3N_4$/N-$CeO_2$ nanocomposites is ascribed to the stretching vibrational frequency of the s-triazine ring pattern in g-$C_3N_4$. Furthermore, the heterocyclic C–N bond has a faint intensity band at 1621 $cm^{-1}$. In addition the aromatic C-N bond vibrations are seen at several transmittance ranges, including 1246, 1423, and 1599 $cm^{-1}$ (Liu et al., 2008). Stretching vibrations of the O–H and N–H are present in representative region like 3000–3600 $cm^{-1}$ range (Fig. 7) (Liu et al., 2015). Finally, the FT-IR spectrum revels that the effective fabrication observed between g-$C_3N_4$ and N-$CeO_2$, which is also confirming formation of g-$C_3N_4$/N-$CeO_2$ nanocomposites by the existence of significant functional groups as C–N, s-triazine, O–H, N–H, and Ce–O (Yang et al., 2012). This superior FTIR results of g-$C_3N_4$/N-$CeO_2$ nanocomposites, good greement with XRD results.

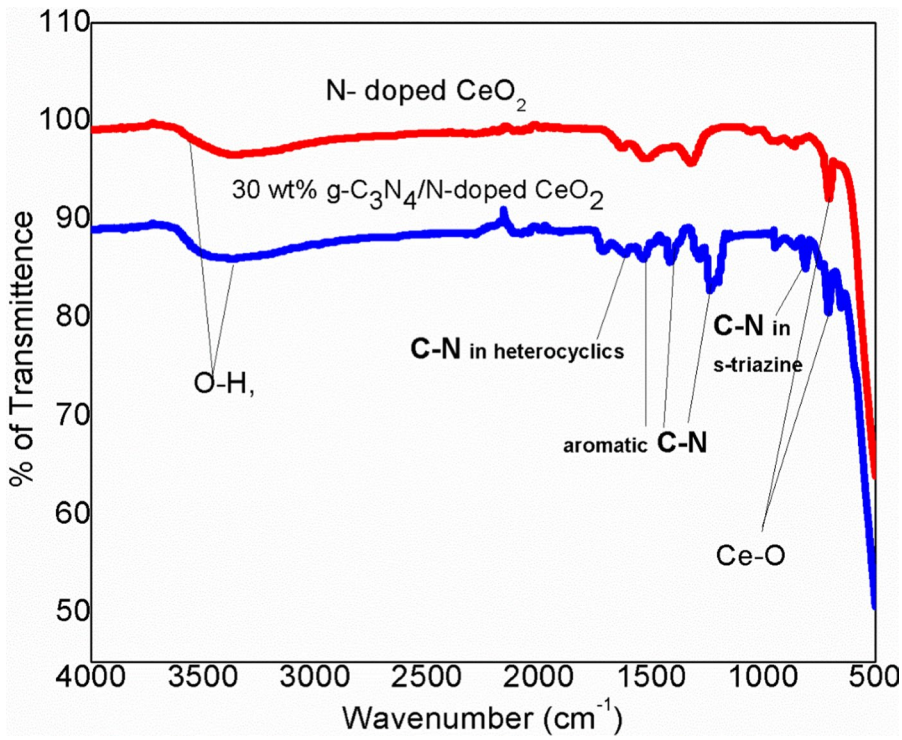


**Fig. 7** FT-IR spectra of N-doped $CeO_2$ nanoparticles and g-$C_3N_4$/N-$CeO_2$ NCs

## Photocatalytic studies

### *Photocatalytic activity of g-$C_3N_4$/N-$CeO_2$ NCs*

Using solar light, photocatalysis offers a potential way to fight water contamination (Nachimuthu et al., 2023). Together with other magnetic exposure to radiation, solar light is composed of around 46% visible light and 4% UV photons. The solar light intensity was measured as $1.20\times10^{-5}$ Einstein $L^{-1}$ $s^{-1}$, which is done by ferrioxalato method. The concentration of degraded dye solution was analysed by UV–visible spectrophotometer in the time interval of 10 min upto 120 min.

Common photocatalysts, such as ZnO, $CeO_2$, and $TiO_2$, primarily absorb UV radiation and have a limited capacity to absorb visible light. Investigators have concentrated on creating nanocomposites that can capture the entire spectrum of solar light in order to overcome this constraint. In keeping with this pattern, we examined the photocatalytic performance of g-$C_3N_4$/N-$CeO_2$ nanocomposites on a model contaminant solution of methylene blue (MB) dye ($\lambda max = 663$ nm) when exposed to solar light (Bai et al., 2014). The photocatalytic breakdown effectiveness of the parent photocatalysts and the g-$C_3N_4$/N-$CeO_2$ nanocomposites during solar light exposure is shown in Fig. 8a.

The decomposition performances of the parent photocatalysts, g-$C_3N_4$ and N-doped $CeO_2$ nanoparticles, for the MB dye are 32% and 40%, respectively, as shown in Fig. 8. On the other hand, the photocatalytic activity of the g-$C_3N_4$/N-$CeO_2$ nanocomposites, which include 10 wt%, 20 wt%, 30 wt%, and 40 wt% g-$C_3N_4$/N-$CeO_2$ NCs, varies from 56 to 97%. Amongst the binary nanocomposites, the 30% g-$C_3N_4$/N-$CeO_2$ NCs exhibit the maximum activity at 97%, which is noteworthy. On the other hand, a modest drop in photocatalytic activity to 75% occurs when the g-$C_3N_4$ level is raised to 40%. Therefore, it is shown that 30% of g-$C_3N_4$ is the ideal concentration for degrading MB dye. The combined g-$C_3N_4$ and N-doped $CeO_2$ nanoparticles in the hybrid structure of g-$C_3N_4$/N-$CeO_2$ NCs lead to an increased degrading effectiveness. By properly separating photogenerated charges, this mixture reduces the rate of recombination. Moreover, the increased rate of deterioration of g-$C_3N_4$/N-$CeO_2$ NCs can be ascribed to their increased surface area and increased absorption of visible light.

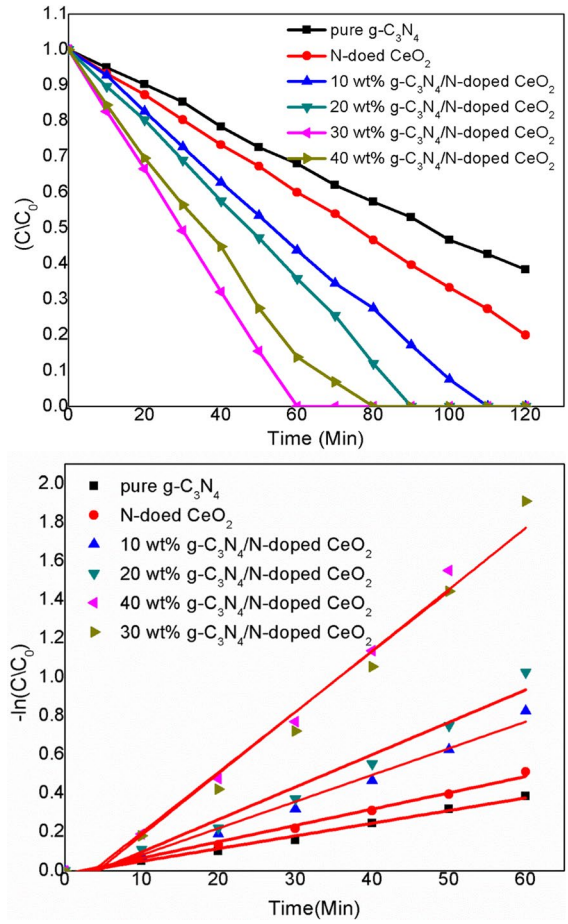


**Fig. 8** Photocatalytic degradation of g-$C_3N_4$/N-$CeO_2$ nanocomposites and its parent photocatalysts

Figure 8b shows the Langmuir–Hinshlwood model (Li et al., 2015) that was used to determine the rate constant k and order of MB dye degradation for g-$C_3N_4$/N-$CeO_2$ NCs. With this approach, a generalized kinetic equation is introduced.

$$\left(-\ln\left(C_t/C_0\right) = k_t\right)$$

where $C_0$ symbolizes the first concentration of dye; $C_t$ is the concentration of dye after *t* minutes of irradiation, and *k* is the rate constant.For g-$C_3N_4$, N-doped $CeO_2$ nanoparticles, and 30%g-$C_3N_4$/N-$CeO_2$ NCs, the computed k values during solar light illumination were around 0.006 $min^{-1}$, 1.28 $min^{-1}$, and

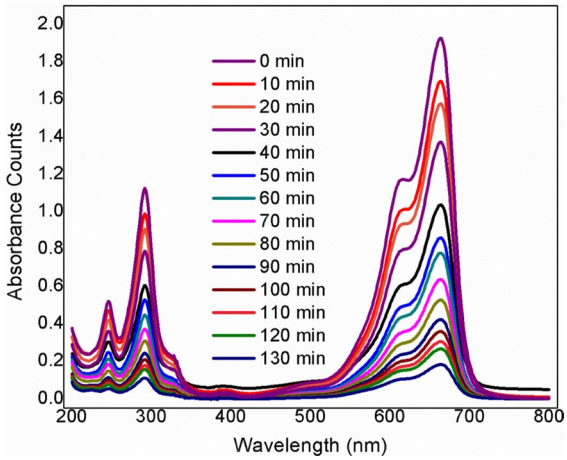


**Fig. 9** Time-dependant UV–visible spectral results of degradation of MB dye presence ofg-$C_3N_4$/N-$CeO_2$ NCs

superior photodegradation efficiency compared to the previously reported catalysts.

Ankit Kumar Singh et al., demonstrate the preparation and application of $NiCo_2O_4$ decorated over a g-$C_3N_4$-based novel nanocomposite ($NiCo_2O_4$@g-$C_3N_4$). $NiCo_2O_4$@g-$C_3N_4$ nanocomposite was employed in the fabrication of a screen-printed carbon electrode-based innovative electrochemical sensing platform and the adsorptive removal of a food dye, i.e., fast green FCF dye (FGD). The adsorption phenomenon of FGD on $NiCo_2O_4$@g-$C_3N_4$ was best fitted ($R^2 = 0.99$) with the Langmuir and Henry model, and the corresponding value of Langmuir adsorption efficiency (qm) was 3.72 mg/g for the removal of FGD within 60 min. Sachin Shoran et al., developed potentials of $CeO_2$/g-$C_3N_4$ (CG) for photocatalytic degradation is

**Table 1** Comparative data of photocatalytic degradation of organic pollutant using g-$C_3N_4$ based nanoparticles

| S. no | Catalyst | Time (min) | Pollutant | Degradation (%) | References |
|---|---|---|---|---|---|
| 1 | $NiCo_2O_4$@g-$C_3N_4$ nanocomposite | 60 | Fast Green Dye | 99 | Ankit Kumar et al. (2023) |
| 2 | $CeO_2$/g-$C_3N_4$ | 90 | rose bengal (RB) and crystal violet (CV) | 97 | Sachin et al. (2023) |
| 3 | $Bi_2MoO_6$/g-$C_3N_4$ binary heterostructure | 160 | Rhodamine-B | 94.6 | Lavanya et al. (2023) |
| 4 | $CeO_2$/g-$C_3N_4$ | 210 | Methylene blue (MB) | 98.5 | Xiaojie et al. (2015) |
| 5 | g-$C_3N_4$/N-$CeO_2$ NCs | **120** | Methylene blue (MB) | **98** | **Herin** |

2.01 $min^{-1}$, respectively. According to our investigation, the degradation rate of g-$C_3N_4$/N-doped $CeO_2$ nanocomposites is much greater than that of N-doped $CeO_2$ nanoparticles.

As shown in Fig. 9, the decomposition performance of g-$C_3N_4$/N-$CeO_2$ NCs was assessed by UV–visible spectrometry under solar light exposure. The capacity of g-$C_3N_4$/N-$CeO_2$ NCs to break down MB dye molecules into mineralized species is shown by these spectrum measurements. Surprisingly, the absorption rate of MB dye gradually drops with sun light being exposed, a sign that macromolecules are breaking down into smaller components.

A comparison of the outstanding photocatalytic degradation efficacy of the g-$C_3N_4$ and $CeO_2$ photocatalyst for the photodegradation of organic pollutant with formerly reported g-$C_3N_4$ and $CeO_2$ based photosystems is compiled in Table 1. It was distinctly noticed that the g-$C_3N_4$ and $CeO_2$ based photosystems in the current study exhibited harmful pollutants into nontoxic compounds without using oxidative agents. The photocatalytic results showed that CG2 effectively degraded rose bengal (RB) and crystal violet (CV) dyes when exposed to visible light irradiation as compared to pure GCN and $CeO_2$. The $Bi_2MoO_6$/g-$C_3N_4$ binary heterostructure is synthesized via a straightforward ultrasonic chemical approach by Amira Masoud et al. The prepared 10% $Bi_2MoO_6$/g-$C_3N_4$ nanocomposite exhibits a significantly improved photocatalytic performance, with a degradation efficiency of 94.6%, (160 min) compared to the single components, $Bi_2MoO_6$ and g-$C_3N_4$, which have degradation efficiencies of only 33% and 31%, respectively. Liying Huang et al., was successfully prepared visible light active Cerium dioxide/graphitic carbon nitride ($CeO_2$/g-$C_3N_4$) by a simple mixing-calcination technique by Liying Huang et al.. The Photocatalytic activities of the $CeO_2$/g-$C_3N_4$ were examined by studying the degradation of methylene

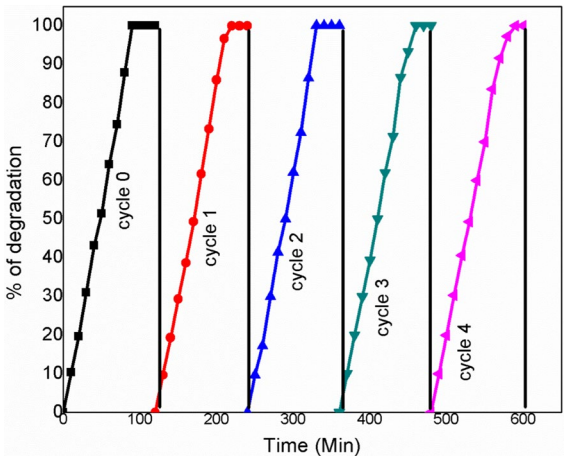


**Fig. 10** Reusability of g-$C_3N_4$/N-$CeO_2$ NCs for five successive cycles

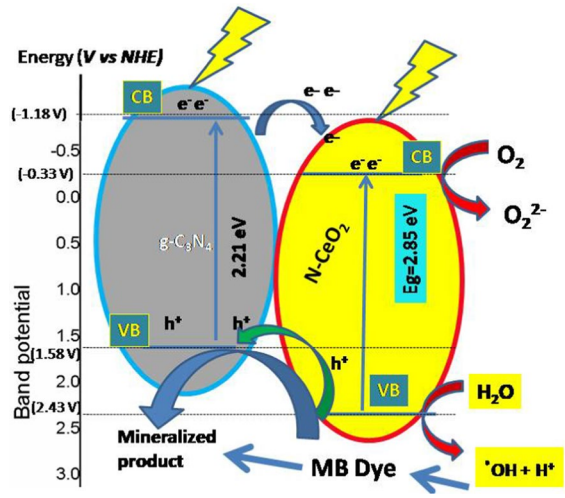


**Fig. 11** Photocatalytic mechanism of g-$C_3N_4$/N doped $CeO_2$ nanocomposites

blue (MB) and 4-chlorophenol (4-CP) under visible light irradiation (> 400 nm). The $CeO_2$/g-$C_3N_4$ composites showed higher photocatalytic activity than that of $CeO_2$ and g-$C_3N_4$. The optimum photoactivity of $CeO_2$/g-$C_3N_4$ exhibited the highest photocatalytic activity within the 70 min. The author revels that enhanced activities could be attributed to the synergetic effect between g-$C_3N_4$ and $CeO_2$.

Effective decomposition processes depend on photocatalysts operating continuously. A substance that produces photons is considered advantageous if it is inexpensive, readily available, and resilient to light exposure. The degrading performance of g-$C_3N_4$/N-$CeO_2$ NCs throughout five successive reuse and recycling operations, each lasting 90 min, is displayed in Fig. 10. After five exposures, there was no discernible decrease in dye degradation, despite small variations. The loss of photocatalyst during handling and centrifugation may be the cause of the modest decrease in degradation effectiveness. These results highlight how important excellent stability as well as effectiveness are for real-world use in photocatalysts.

*Photocatalytic mechanism of g-$C_3N_4$/N-$CeO_2$ NCs*

Figure 11 shows a hypothesized process based on the optical and band arrangement features found in g-$C_3N_4$/N-$CeO_2$ NCs. The following formula determines the locations of the conduction and valence bands in the semiconductor: $E^0_{CB} = E^C - 1\backslash 2\ E_g$, where $\chi$ is the semiconductor's absolute electronegativity (it is 5.56 eV for $CeO_2$). On the hydrogen scale, $E^C$ stands for free electron energy (4.5 eV), and $E_g$ for the photocatalysts band gap energy. N-doped $CeO_2$ band gap was found to be 2.85 eV based on the findings of the band gap measurement.

N-doped $CeO_2$ nanoparticles have calculated valence band (VB) and conduction band (CB) potentials of 2.43 V and − 0.33 V, respectively. On the other hand, g-$C_3N_4$ displays a CB bottom at − 1.18 V and a maximal VB parabola at 1.58 eV. g-$C_3N_4$ has a CB potential of − 1.18 eV, which is significantly smaller than the CB potential of N-doped $CeO_2$ nanoparticles (− 0.33 eV). This implies that photogenerated holes on N-doped $CeO_2$ nanoparticles may move to g-$C_3N_4$ across the formed interface, whereas excited electrons at the CB of g-$C_3N_4$ could migrate to the CB of N-doped $CeO_2$ nanoparticles. As a result, this technique may be able to decrease charge recombination and increase the efficiency of photocatalytic reactions.

*Reactive species studies*

We carried out a reactive species quenching investigation in order to understand the degradation process of dyes based on MB, as shown in Fig. 12. The g-$C_3N_4$/N-$CeO_2$ NCs potent contact between g-$C_3N_4$ and N-doped $CeO_2$ prevents electron–hole recombination, which boosts the activity of dye degradation. Active radicals such as superoxide, holes, and

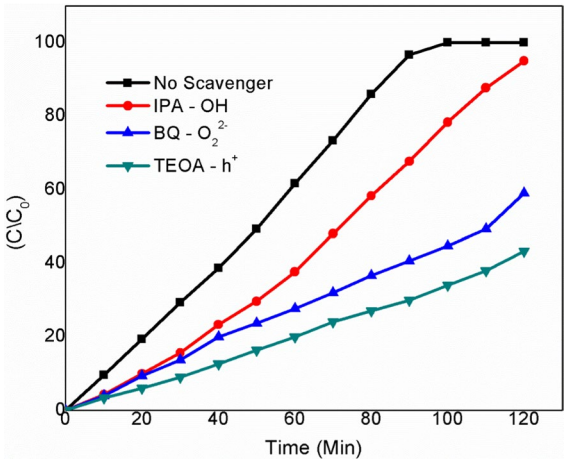


**Fig. 12** Scavenging activity of g-$C_3N_4$/N-$CeO_2$ NCs

hydroxyl radicals are essential for the photocatalytic destruction of organic pollutants. This was investigated by using benzoquinone (BQ), triethanolamine (TEOA), and isopropyl alcohol (IPA) as harvesters for hydroxyl, hole, and superoxide radicals, respectively. Out of all the nanocomposites that were evaluated, 30 wt% g-$C_3N_4$/N-$CeO_2$ NCs showed the best photocatalytic effectiveness and were chosen for the scavenging investigation.

Even in the absence of scavenging components, the 30 wt% g-$C_3N_4$/N-$CeO_2$ NCs demonstrated remarkable photocatalytic efficacy, degrading MB dye by 96.6% in just 90 min of being exposed to sun light. In contrast, the degradation efficacy dropped to 90.6%, 58.7%, and 43.29%, respectively, after scavengers such IPA, TEOA, and BQ were added to the photocatalytic solution. This decrease indicates that the main active species causing the decomposition processes are superoxide radicals and holes, with TEOA and BQ significantly reducing the efficacy by about 41.3% and 56.7%, respectively.

## Conclusion

The desired outcome of this work is to combine g-$C_3N_4$ sheets with N-doped $CeO_2$ nanoparticles to create g-$C_3N_4$/N-doped $CeO_2$ nanocomposites. It has been verified that these nanocomposites successfully formed using a variety of characterisation methods, including PXRD, FT-IR, SEM, and TEM. Particularly, the nanocomposites enhanced absorption of visible light is demonstrated by the UV–visible DRS spectra. Effective charge separation is suggested by PL analysis, which lowers electron–hole recombination. Significantly, as compared with individual catalysts, the nanocomposites show improved MB dye degradation in the presence of solar irradiation. Their enhanced catalytic activity is further supported by photostability experiments and investigations on radical scavenging. These composite materials exceptional effectiveness can be attributed to their unique physicochemical characteristics, which have been extensively studied. Through the combined benefits of g-$C_3N_4$ and N-doped $CeO_2$, these novel binary composites show great potential for a variety of uses for ecological remediation and transformation of energy.

**Acknowledgements** The authors express their sincere appreciation to the Researchers Supporting Project Number (RSP2024R398) King Saud University, Riyadh, Saudi Arabia

**Author contributions** A. S. Karthik: Conceptualization, Methodology, Writing- Original draft preparation. Smita Agrawal: Data curation, Writing. S. Senthil: Conceptualization, Methodology, Writing- Original draft preparation. Abhijit Debnath: Visualization, Investigation. Sandhanasamy Devanesan: Visualization, Investigation. Ahmed. E. A. Zohier: Reviewing and Editing. S. Vignesh: Visualization, Investigation. All authors reviewed the manuscript.

**Funding** I haven't acquired any financial support.

**Data availability** The corresponding author can provide access to the datasets generated or analyzed during the current study upon reasonable request.

**Declarations**

**Conflict of interest** The authors declare that they have no known competing financial interests or personal relationships that could have appeared to influence the work reported in this paper.

**Ethical approval** This declaration does not apply in this context.

## References

Abbasi, Z., Haghighi, M., Fatehifar, E., & Rahemi, N. (2012). Comparative synthesis and physicochemical characterization of $CeO_2$ nanopowder via redox reaction, precipitation and sol–gel methods used for total oxidation of toluene.

*Asia-pacific Journal of Chemical Engineering, 7*, 868. https://doi.org/10.1002/apj.652

Akpan, U. G., & Hameed, B. H. (2009). Parameters affecting the photocatalytic degradation of dyes using $TiO_2$-based photocatalysts: A review. *Journal of Hazardous Materials, 170*, 520. https://doi.org/10.1016/j.jhazmat.2009.05.039

Ankit Kumar, S., Shreanshi, A., Ravindra Kumar, G., & Ida, T. (2023). A highly efficient $NiCo_2O_4$ decorated g-$C_3N_4$ nanocomposite for screen-printed carbon electrode based electrochemical sensing and adsorptive removal of fast green dye. *Environmental Science and Pollution Research*. https://doi.org/10.1007/s11356-023-30373-3

Bai, X., Zong, R., Li, C., Liu, D., Liu, Y., & Zhu, Y. (2014). Enhancement of visible photocatalytic activity via Ag@$C_3N_4$ core–shell plasmonic composite. *Applied Catalysis b: Environmental, 147*, 82. https://doi.org/10.1016/j.apcatb.2013.08.007

Chandrasekar, N., Steffi, A. P., Ramachandran, B., Hwang, M. T., Faramarzi, V., & Govarthanan, M. (2023). MXenes–Versatile 2D materials for identification of biomarkers and contaminants in large scale environments: A review. *Environmental Research, 228*, 115900.

Dey, N., Vickram, S., Thanigaivel, S., Kamatchi, C., Subbaiya, R., Karmegam, N., & Govarthanan, M. (2022). Graphene materials: Armor against nosocomial infections and biofilm formation—A review. *Environmental Research, 214*, 113867.

Divya, G., Sivakumar, S., Sakthi, D., Priyadharsan, A., Arun, V., Kavitha, R., & Boobas, S. J. (2021). Developing the NiO/$CuTiO_3$/ZnO ternary semiconductor heterojunction for harnessing photocatalytic activity of reactive dye with enhanced durability. *Journal of Inorganic and Organometallic Polymers and Materials, 31*, 4480. https://doi.org/10.1007/s10904-021-02068-0

Gao, P., Liu, J., Sun, D. D., & Ng, W. (2013). Graphene oxide–CdS composite with high photocatalytic degradation and disinfection activities under visible light irradiation. *Journal of Hazardous Materials, 15*, 412. https://doi.org/10.1016/j.jhazmat.2013.02.003

Gomathi, A., Priyadharsan, A., Prabhuraj, T., Vasanthi, G., Gokilapriya, S., & Ramesh Kumar, K. A. (2023). Boosting the performance of solar light driven $CeO_2$/$BiVO_4$ anchored g-$C_3N_4$ nanocomposites: A systematic study toward the development of a photocatalytic and antibacterial activity. *Colloids and Surfaces a: Physicochemical and Engineering Aspects, 673*, 131835. https://doi.org/10.1016/j.colsurfa.2023.131835

Huang, B., He, J., Bian, S., Zhou, C., Li, Z., Xi, F., Liu, J., & Dong, X. (2018). S-doped graphene quantum dots as nanophotocatalyst for visible light degradation. *Chinese Chemical Letters, 29*, 1698. https://doi.org/10.1016/j.cclet.2018.01.004

Lavanya, G., Anandaraj, K., Gopu, M., Selvam, K., Selvankumar, T., Govarthanan, M., & Kumar, P. (2023). Green chemistry approach for silver nanoparticles synthesis from *Halimeda macroloba* and their potential medical and environmental applications. *Applied Nanoscience, 13*(9), 5865–5875.

Li, D., Yang, K., Wang, X., Ma, Y., Huang, G., & Huang, W. (2015). Origin of enhanced visible-light photocatalytic activity of transition-metal (Fe, Cr and Co)-doped $CeO_2$: Effect of 3d orbital splitting. *Applied Physics A, 120*, 1205. https://doi.org/10.1007/s00339-016-0700-9

Li, X. F., Zhang, J., Shen, L. H., Ma, Y. M., Lei, W. W., Cui, Q. L., & Zou, G. T. (2009). Preparation and characterization of graphitic carbon nitride through pyrolysis of melamine. *Applied Physics a: Materials Science and Processing, 94*, 387. https://doi.org/10.1007/s00339-008-4816-4

Liu, L., Ma, D., Zheng, H., Li, X. J., Cheng, M. J., & Bao, X. H. (2008). Synthesis and characterization of microporous carbon nitride. *Microporous and Mesoporous Materials, 110*, 216. https://doi.org/10.1016/j.micromeso.2007.06.012

Liu, Y., Wang, R., Yang, Z., Du, H., Jiang, Y., & Shen, C. (2015). Enhancement of catalytic activity and oxidative ability for graphitic carbon nitride. *Chinese Journal of Catalysis, 36*, 2135. https://doi.org/10.1016/j.jphotochemrev.2016.06.001

Liying, H., Yeping, L., Xu, H., Yuanguo, Xu., Xia, J., Kun, W., Huaming, L., & Xiaonong, C. (2013). Synthesis and characterization of $CeO_2$/g-$C_3N_4$ composites with enhanced visible-light photocatatalytic activity. *RSC Advances, 3*(44), 22269. https://doi.org/10.1039/c3ra42712a

Malathi, A., Priyadharsan, A., Handayani, M., Hasan, I., Divya, G., Sivaranjani, K., & Sivakumar, S. (2024). Boosted solar-driven photocatalysis: Silver molybdate/reduced graphene oxide nanocomposites for methylene blue decomposition. *Ionics, 30*(3), 1–12. https://doi.org/10.1007/s11581-023-05346-8

Malathi, A., Priyadharsan, A., Ragupathy, S., Sivakumar, S., Vadivel, P., Arun, V., Sivakumar, M., & Sakthi, D. (2023). Enhanced sun light driven photocatalytic activity of silver tungstate/reduced graphene oxide nanocomposites for methylene blue dye degradation. *Journal of Inorganic and Organometallic Polymers and Materials*. https://doi.org/10.1007/s10904-023-02887-3

Malathy, A., Manikandan, V., Sandhanasamy, D., Karim, F., Priyadharsan, A., Ragavendran, C., Ragupathy, S., Ranjith, R., & Sivakumar, S. (2023). Development of biohybrid $Ag_2CrO_4$/rGO based nanocomposites with stable flotation properties as enhanced photocatalyst for sewage treatment and antibiotic-conjugated for antibacterial evaluation. *International Journal of Biological Macromolecules, 244*, 125303. https://doi.org/10.1016/j.ijbiomac.2023.125303

Manimegalai, S., Vickram, S., Deena, S. R., Rohini, K., Thanigaivel, S., Manikandan, S., Subbaiya, R., Karmegam, N., Kim, W., & Govarthanan, M. (2023). Carbon-based nanomaterial intervention and efficient removal of various contaminants from effluents: A review. *Chemosphere, 312*, 137319.

Muthamilarasu, A., Divya, G., Sivakumar, M., Sakthi, D., & Sivakumar, S. (2022). NiO/CuO/$TiO_2$ ternary composites: Development, physicochemical characterization and photocatalytic degradation study over reactive orange 30 solutions under solar light irradiation. *Advances in Material Science, 22*, 71. https://doi.org/10.2478/adms-2022-0003

Nachimuthu, V., Amirthalingam, M., Govindhasamy, M., Palanisamy, S., Ashraf, A. H., Bassam, K. A., Manavalan, R. K., & Shaik, G. P. P. S. (2023). Visible light active hybrid silver decorated g-$C_3N_4$–$CeO_2$ nanocomposite for

ultrafast photocatalytic activity and toxicity evaluation. *Environmental Research, 216*, 114749. https://doi.org/10.1016/j.envres.2022.114749

Nas, M. S., Calimli, M. H., Burhan, H., Yilmaz, M., Mustafov, S. D., & Sen, F. (2019). Synthesis, characterization, kinetics and adsorption properties of Pt-Co@GO nano-adsorbent for methylene blue removal in the aquatic mediums using ultrasonic process systems. *Journal of Molecular Liquids, 296*, 112100. https://doi.org/10.1016/j.molliq.2019.112100

Rajendran, R., Rojviroon, O., Arumugam, P., Natchimuthu, K., Vasudevan, V., Kannupaiyan, J., Muangmora, R., Phouheuanghong, P., & Rojviroon, T. (2024). Design and fabrication of g-$C_3N_4$/$Bi_2S_3$ heterojunction photocatalysts for efficient organic pollutant degradation and antibacterial activity. *Journal of Alloys and Compounds, 976*, 173116. https://doi.org/10.1016/j.jallcom.2023.173116

Rajendran, R., Vignesh, S., Balachandar, R., Suganthi, S., Raj, V., Ramasundaram, S., Jeyaperumal, K. S., Shkir, M., & Oh, T. (2022). Construction of novel g-$C_3N_4$ coupled efficient $Bi_2O_3$ nanoparticles for improved Z-scheme photocatalytic removal of environmental wastewater contaminant: Insight mechanism. *Journal of Environmental Management, 330*, 117134. https://doi.org/10.1016/j.jenvman.2022.117134

Ran, M., Sai, Z., Lei, L., Pengcheng, G., Tao, W., Ayub, K., Shaojun, L., Bingfeng, L., Suhua, W., & Xiangke, W. (2019). Enhanced visible-light-induced photoactivity of type-II $CeO_2$/g-$C_3N_4$ nanosheet toward organic pollutants degradation. *ACS Sustainable Chemistry & Engineering, 7*, 9699. https://doi.org/10.1021/acssuschemeng.9b01477

Ranjith, R., Karmegam, N., Alsawalha, M., Xuefeng, Hu., & Jothimani, K. (2023). Construction of g-$C_3N_4$/CdS/$BiVO_4$ ternary nanocomposite with enhanced visible-light-driven photocatalytic activity toward methylene blue dye degradation in the aqueous phase. *Journal of Environmental Management, 330*, 117132. https://doi.org/10.1016/j.jenvman.2022.117132

Ratchnashree, S. R., Karmegam, N., Selvam, M., Manikandan, S., Deena, S. R., Subbaiya, R., Vickram, A. S., Kim, W., & Govarthanan, M. (2023). Advanced technologies for the determination of quantitative structure-activity relationships and degradation efficiency of micropollutants and their removal in water: A review. *Science of the Total Environment, 904*, 166563.

Runda, H., Jing Wu, M. Z., Baiquan, L., Zhaoqiang, Z., & Dongxiang, L. (2021). Strategies to enhance photocatalytic activity of graphite carbon nitride-based photocatalysts. *Materials & Design, 210*, 110040. https://doi.org/10.1016/j.matdes.2021.110040

Sachin, S., Sudesh, C., & Anshu, S. (2023). Photocatalytic dye degradation and antibacterial activities of $CeO_2$/g-$C_3N_4$ nanomaterials for environmental applications. *Environmental Science and Pollution Research, 30*(44), 98682–98700. https://doi.org/10.1007/s11356-022-23815-x

Thangavelu, K., Rajendran, R., Palanisamy, S., Arumugam, P., & Thammasak, R. (2023). Powerful combination of $FeWO_4$/g-$C_3N_4$ heterostructures for solar light driven photocatalytic degradation of tetracycline and its antibacterial activity. *Materials Today Sustainability, 24*, 100562. https://doi.org/10.1016/j.mtsust.2023.100562

Wang, J., Zhu, M., Chen, Z., Chen, Y., Hayat, T., Alsaedi, A., & Wang, X. (2019). Polyacrylamide modified molybdenum disulfide composites for efficient removal of graphene oxide from aqueous solutions. *Chemistry Engineering Journal, 361*, 651. https://doi.org/10.1016/j.cej.2018.12.123

Wetchakun, N., Chaiwichain, S., Inceesungvorn, B., Pingmuang, K., Phanichphant, S., & Minett, A. I. (2012). $BiVO_4$/$CeO_2$ nanocomposites with high visible-light-induced photocatalytic activity. *ACS Applied Materials & Interfaces, 4*, 3718. https://doi.org/10.1021/am300812n

Xiaojie, S., Hui, X., Hefei, W., Jiexiang, X., Yanhua, S., Jia, Y., Yuanguo, X., Qi, Z., Daolin, D., Huaming, L. (2015). Controllable synthesis of $CeO_2$/g-$C_3N_4$ composites and their applications in the environment. *Dalton Transactions*, *44*(15), 7021–7031. https://doi.org/10.1039/C4DT03793F

Xiaolong, D., Chenggang, W., Hongcen, Y., Minghui, S., Shouwei, Z., Xiao, W., Meng, D., Jinzhao, H., & Xijin, X. (2017). One-pot hydrothermal synthesis of CdS decorated CuS microflower-like structures for enhanced photocatalytic properties. *Scientific Reports, 7*, 1. https://doi.org/10.1038/s41598-017-04270-y

Xu, H., Xu, Y., Li, H., Xia, J., Xiong, J., Yin, S., Huang, C., & Wan, H. (2012). Synthesis, characterization and photocatalytic property of AgBr/$BiPO_4$ heterojunction photocatalyst. *Dalton Transactions, 41*, 3387. https://doi.org/10.1039/C2DT11969B

Yang, M., Huang, Q., & Jin, X. (2012). Visible light-induced Cr-doped $SrTiO_3$-g-$C_3N_4$ composite for improved photocatalytic performance. *Materials Science and Engineering: B, 177*, 600. https://doi.org/10.1007/s11595-014-1051-z

Zhiquan, H., Leicheng, L., Zhiping, L., Huan, L., & Jiaqi, W. (2020). Synthesis of novel kaolin-supported g-$C_3N_4$/$CeO_2$ composites with enhanced photocatalytic removal of ciprofloxacin. *Materials, 13*, 3811. https://doi.org/10.3390/ma13173811